Triacylphosphines as a Novel Class of Phosphorus Sources for the Synthesis of Transition Metal Phosphide Nanoparticles

Artsiom Antanovich,[1,2*] Andrey Iodchik,[1] Jing Li,[1] Pavel Khavlyuk,[1] Volodymyr Shamraienko,[1] Vladimir Lesnyak[1,*]

[1]Physical Chemistry, TU Dresden, Zellescher Weg 19, 01069 Dresden, Germany

[2]Institute of Physical Chemistry and Electrochemistry, Leibniz University Hannover, Callinstraße 3a, D-30167 Hannover, Germany

Abstract

Transition metal phosphide (TMP) nanoparticles (NPs) are versatile materials for energy conversion/storage applications due to their robustness and many possibilities to tailor NPs' electronic, physical, and chemical properties. One of the hurdles towards their broader implementation is their challenging synthesis exacerbated by the limited choice of phosphorus precursors. On the one hand, the synthesis of TMP NPs can employ various alkyl- or arylphosphines requiring prolonged heating at high temperatures, while on the other hand, highly reactive $P(SiMe_3)_3$, white phosphorus, or PH_3 pose additional obstacles associated with their hazardous nature, high cost, and limited availability. This work introduces the use of acylphosphines as a new class of phosphorus sources for synthesizing phosphide NPs. They were shown to react with respective metal chlorides at moderate temperatures as low as 250 °C yielding poorly crystalline NPs, which can later be crystallized at 305 °C. After ligand stripping with HPF_6, NPs were found to be an effective electrocatalyst for the hydrogen evolution reaction in the acidic medium exhibiting overpotentials as low as 50 mV at a current density of 10 mA/cm^2, which is among the lowest overpotentials for these materials and is quite competitive to commercial platinum-based catalysts.

1. Introduction

Over the last decade transition metal phosphide (TMP) nanoparticles (NPs) have emerged as a material of interest for a variety of energy conversion/storage applications, such as electrical capacitors,[1,2] thermoelectrics,[3] ion batteries,[4] etc. To date, there have been many reports on the synthesis of phosphides of nickel,[5–10] cobalt,[8,9,11–13] iron,[8,14–17] molybdenum,[18–20] copper,[21–24] manganese,[25–27] tungsten,[28] etc.

One of the important rapidly developing research avenues for this class of materials is their application in various catalytic processes including photocatalysis,[29,30] organic catalysis,[31–34] electrocatalysis for CO_2-conversion,[35–39] hydrogen and oxygen evolution.[40–48] Over the years, their catalytic performance characteristics have been steadily approaching those of state-of-the-art systems

based on noble metals. In addition, TMPs comprise widely abundant elements, which drastically reduces the cost of their large-scale implementation.[41,49–51] Moreover, many TMPs exhibit excellent robustness and broad flexibility of their physical, chemical, and electronic properties due to a vast number of available stoichiometries, and crystal structures, which can be further modified by alloying, doping, as well as size- and shape-control.

One of the main obstacles hindering the development of TMP catalysts is their challenging synthesis due to the strong metal-phosphorus and covalent phosphorus-phosphorus bonds, which usually require harsh reaction conditions and an appropriate phosphorus source, the range of which remains severely limited.[52] Often, such NPs are prepared on various supports at high (> 500 °C) temperatures,[53,54] which greatly increases the required energy input. The introduction of colloidal syntheses in solution helped resolve this issue and opened new possibilities to manipulate the properties of TMP NPs. The majority of works reported so far utilized either trialkyl- or triarylphosphines (e.g. trioctylphosphine)[5–7,11–14,16,21,26] and related metal complexes,[55,56] organophosphites[8–10] or aminophosphines[57–59] as a phosphorous source in combination with metal acetates,[5,23,27] chlorides,[8,19,21] acetylacetonates,[6,7,11] oxides,[15] carbonyls,[12,14,16,25,26] bulk or nanosized metals[13] at elevated temperatures.[41] However, due to the low reactivity of these phosphorus sources, the synthesis protocols still require keeping the reaction at high temperatures (albeit significantly lower than previous approaches – 300-360 °C) for prolonged periods of time and the use of large amounts of stabilizing agents such as fatty amines[5–8,13,14,16,21] or fatty acids[11,12,25]. On the other side of the reactivity spectrum are $P(SiMe_3)_3$,[25,60] white phosphorus,[61,62] and PH_3 gas,[63,64] but they pose significant hazards due to their high flammability and toxicity as well as high cost.

In this work, we report the high yield and purity synthesis of acylphosphines employing inexpensive starting materials. Using tributyrylphosphine ($(PrCO)_3P$) and tribenzoylphosphine (Bz_3P) as a case study, for the first time we demonstrate their utility as a new class of reactive phosphorus precursors for the preparation of nickel, cobalt, iron, and molybdenum phosphides at moderate (250-305 °C) temperatures. We demonstrate that the size and crystallinity degree of resulting metal phosphide NPs can be controlled by the synthesis temperature and the type of acyl substitutes of the phosphine. Finally, we studied the performance of the ligand-exchanged TMP NPs as electrocatalysts for hydrogen evolution reaction (HER) in the acidic and basic media. We show that among the studied TMP NPs the lowest HER overpotential of 50 mV at 10 mA/cm^2 and a small Tafel slope of 46 mV/dec were achieved by $Ni_2P/Ni_{12}P_5$ NPs in acidic media, which are among the best values demonstrated by non-noble metal-based TMP NPs reported to date.

2. Results and discussion

$(PrCO)_3P$ and Bz_3P were synthesized by the acylation of sodium dihydrogenphosphide prepared by the protonation of sodium phosphide with *t*-BuOH (**Scheme 1**). The composition and structure of these compounds were confirmed by elemental analysis and NMR-spectra (**Figure S1** in the Supporting Information), which were consistent with the literature data.[65,66] Both phosphines were isolated with high (> 50 %) reaction yields and purity and were found to be soluble in THF, DME, $CHCl_3$, and toluene. In addition, $(PrCO)_3P$ is soluble in hexane and octadecene-1 (ODE). When exposed to air, $(PrCO)_3P$ reacts exothermically producing white fumes, while Bz_3P was found to be relatively stable.

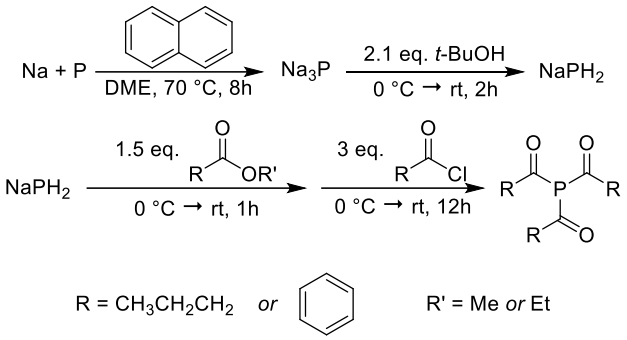

Scheme 1. Synthesis scheme of $(PrCO)_3P$ and Bz_3P.

Metal phosphide NPs were synthesized by reacting metal chlorides with either $(PrCO)_3P$ or Bz_3P as a phosphorus precursor in ODE. To investigate the reactivity of the prepared phosphines we used the heat-up approach widely applied in the synthesis of TMP NPs. During the preliminary experiments the phosphines were found to be unreactive towards nickel and cobalt oleates in ODE prior to their decomposition; $(PrCO)_3P$ quickly decomposed when using respective chlorides in oleylamine, whereas Bz_3P was more stable but led to the low yield and irregular shaped NPs. Thus, instead, we opted to perform the synthesis in ODE using trioctylphosphine (TOP) as a metal complexing agent facilitating the dissolution of respective chlorides. After the dissolution of metal precursors, the acylphosphines were injected at 90 °C into the reaction mixture, which was then heated to the required temperature (250 – 305 °C). Upon heating the reaction mixture began darkening at ca. 150 °C and 170 °C in the case of $NiCl_2$ and $CoCl_2$, respectively, indicating the reaction between acylphosphines and metal salts and kept turning black over the reaction progress.

Figure 1 shows transmission electron microscopy (TEM) images and X-ray diffraction (XRD) patterns of nickel phosphide NPs prepared using the synthesized acylphosphines. One can see that at 250 °C both phosphorus sources yield small (5 ± 1 nm and 4 ± 0.5 nm, in the case of Bz_3P and $(PrCO)_3P$, respectively) quasi-spherical NPs. Corresponding XRD patterns exhibit significantly broadened low-intensity reflexes attributed to the hexagonal Ni_2P phase consistent with small-sized poorly crystalline NPs. When the synthesis temperature was increased to 305 °C, the size of obtained

NPs increased to 8.5 ± 1.5 nm and 7.5 ± 1.5 nm in the case of Bz_3P and $(PrCO)_3P$, respectively, while the XRD reflections became more pronounced, in line with previous reports suggesting that TMP NPs require high temperature to crystallize.[8,67,68] It is worth mentioning that higher temperatures resulted in higher NP yields indicating that crystallization was accompanied by further monomer conversion facilitating the size increase.

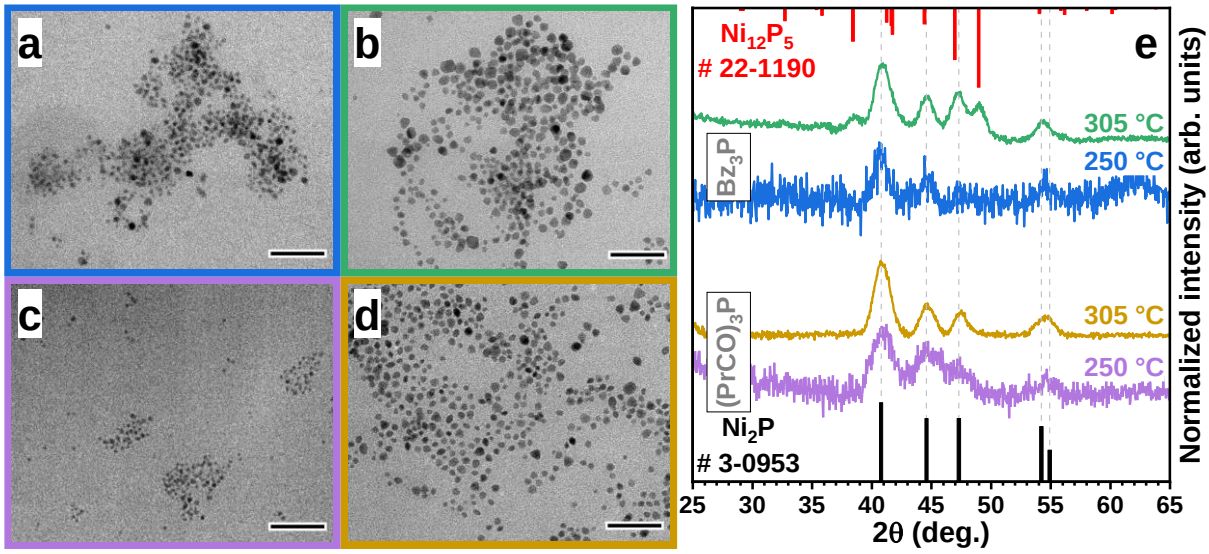

Figure 1. TEM images (a–d) and XRD patterns (e) of nickel phosphide NPs synthesized using Bz_3P at 250 °C (a) and 305 °C (b), and $(PrCO)_3P$ at 250 °C (c) and 305 °C (d). Scale bars in TEM images are 50 nm. Dashed lines in (e) correspond to the XRD pattern of hexagonal Ni_2P (# 3-0953) and serve as a guide for an eye

Furthermore, nickel phosphide NPs prepared with Bz_3P at 305 °C exhibit additional reflections at 38.5° and 49.0° attributable to the metal-rich tetragonal $Ni_{12}P_5$ phase. Its formation might be explained by the lower reactivity of the acylphosphine as suggested by its aforementioned stability towards air exposure and its higher thermal stability.[66] Considering the mechanistic speculations above, lower reactivity results in a smaller yield of poorly crystalline intermediates leaving more unreacted nickel salt in solution, creating more metal-rich conditions for later reaction stages, which were previously reported to facilitate the formation of $Ni_{12}P_5$ NPs.[7] This assumption is also in line with the slightly bigger size of NPs prepared with Bz_3P, since slower monomer flux generally facilitates the growth of NPs to larger sizes.

In a similar manner to nickel phosphide, we also synthesized cobalt phosphide NPs using cobalt dichloride as a metal source. Cobalt precursor was found to be slightly less reactive towards acylphosphines, thus low-temperature cobalt phosphide was prepared at 275 °C. TEM images and corresponding XRD patterns of the prepared cobalt phosphide NPs are displayed in **Figure 2**.

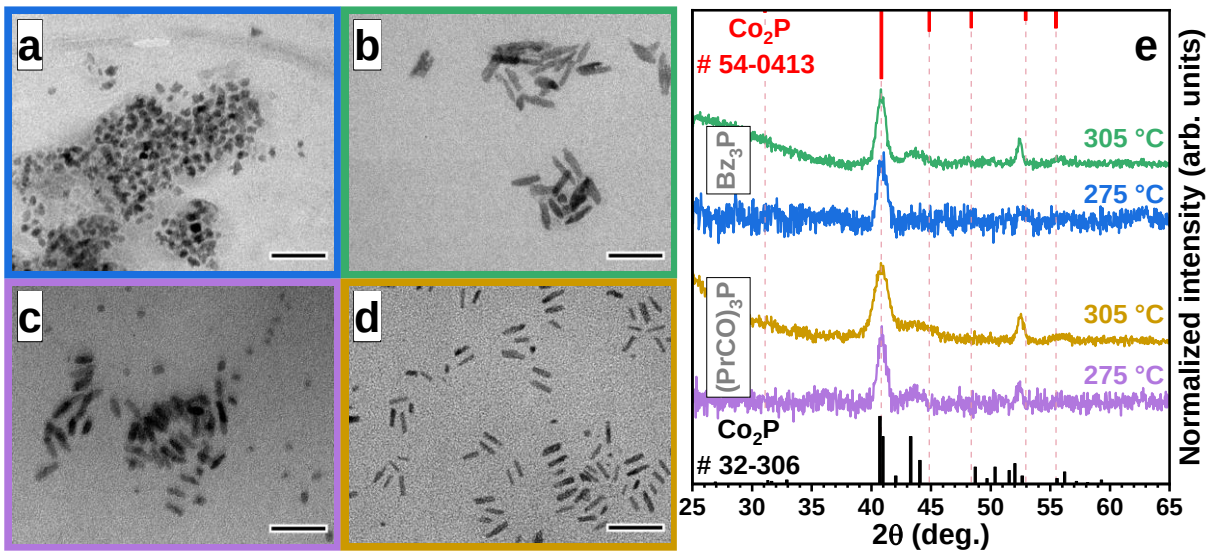

Figure 2. TEM images (a-d) and XRD patterns (e) of cobalt phosphide NPs synthesized using Bz_3P at 275 °C (a) and 305 °C (b), and $(PrCO)_3P$ at 275 °C (c) and 305 °C (d). Scale bars in TEM images are 50 nm. Dashed lines in (e) correspond to the XRD pattern of hexagonal Co_2P (# 54-0413) and serve as a guide for an eye.

As in the case of Ni phosphides, cobalt phosphide NPs synthesized using Bz_3P at the lower temperature are quasi-spherical albeit having rougher surfaces with average sizes of 9 ± 1.5 nm. At the same time, in the case of $(PrCO)_3P$) a mixture of rod-like (length 19.0 ± 2.5 and width 7.5 ± 1.0 nm) and quasi-spherical NPs (7.5 ± 2 nm) was observed (**Figure 2c** and **Figure S2** in the Supporting Information). In both cases, respective XRD patterns exhibit low-intensity reflections of orthorhombic Co_2P. The syntheses at the higher temperature resulted in cobalt phosphide NPs with markedly different shapes of nanorods with dimensions of 18 ± 3 nm × 5 ± 1 nm and 29 ± 4.5 nm × 6.5 ± 1 nm when using $(PrCO)_3P$ and Bz_3P, respectively. Notably, the diameter of cobalt phosphide nanorods is smaller than the diameter of quasi-spherical NPs prepared at lower temperatures, indicating that some recrystallization of smaller NPs takes place at higher temperatures, which is consistent with the NP growth mechanistic speculations above. Similarly to Ni phosphides, the increase of the synthesis temperature also higher NP crystallinity as evidenced by a higher intensity of XRD reflections and the appearance of additional reflection at ~52.4°.

It is worth mentioning that TMP NPs prepared with alkyl- or arylphosphines in metal-rich conditions often exhibit hollow structures due to the two-step reaction mechanism involving phosphidation of intermediate metallic NPs leading to the appearance of voids due to the Kirkendall effect.[12,67–70] The formation of holes in NPs can be suppressed by significantly increasing the ratio of alkylphosphines above ca. 9-fold excess of phosphorus precursor, which pushes the reaction towards the formation of amorphous metal phosphide NPs.[67,68] In our case, particles appear solid and homogeneous and we observed no signs of the formation of metallic NPs at any point of the

reaction via XRD or TEM analysis. This suggests that even in metal-rich conditions acylphosphines with a molecular structure similar to the abovementioned alkyl- or arylphosphines react with metal salts, first forming molecular metal-acylphosphine complexes[71] (as suggested by the color change of the reaction mixture), which then undergo the intermolecular rearrangement similar to the reaction mechanism reported for organophosphites.[10] Considering that alkylphosphines are known to efficiently catalyze acylation reactions, aside from being a co-solvent and a ligand TOP can also facilitate complex decomposition through the nucleophilic attack of the carbonyl group.[72,73] This reaction results in the formation of respective poorly crystalline or amorphous phosphide NPs, which later recrystallize and provide the flux of monomers for further NP growth, explaining the larger sizes and the shape change of NPs prepared at higher temperatures. Together with somewhat lower reaction temperatures, this suggests that the introduction of the carbonyl group in the vicinity of the central phosphorus atom significantly improves the reactivity of phosphines.

Furthermore, we also examined the reactivity of the prepared phosphines towards copper (I), iron (II), and molybdenum (V) chlorides. In the case of copper and iron, TEM imaging reveals the formation of very large crystalline NPs of the respective phosphides with sizes on the scale of hundreds of nm (see **Figure S3** in the Supporting Information). Such drastic size difference can be most likely attributed to the poor ability of chloride and TOP to passivate the surface of the formed metal phosphide NPs, resulting in their uncontrolled growth. Conversely, the reaction with molybdenum (V) chloride yielded very small (~2 nm) amorphous NPs with poorly defined shapes (see **Figure S3 d,h** in the Supporting Information). It is worth mentioning that crystalline molybdenum phosphide is notoriously hard to prepare via the synthesis in solution since its crystallization requires temperatures well above 305 °C and is usually conducted as an additional annealing step.[8,18]

Since both acylphosphines and TOP can potentially act as a phosphorus source for TMP NPs, to verify whether $(PrCO)_3P$ and Bz_3P are indeed playing the major role in the reaction, we performed additional syntheses in the same manner, except for the injection of the acylphosphines. In the case of cobalt and nickel chlorides, the reaction resulted in respective phosphide NPs with poor chemical yield, however, their TEM images are markedly different from the ones shown above, demonstrating particles with significantly larger sizes of tens of nm (**Figure S4** in the Supporting Information). In the case of copper, iron, and molybdenum chlorides, no reaction was observed even after the prolonged heating at 305 °C.

Next, we evaluated the electrocatalytic performance of the synthesized NPs deposited onto the glassy carbon electrode in both acidic (0.5 M H_2SO_4) and alkaline (1 M KOH) aqueous solutions. Since NPs synthesized in the organic medium are sterically stabilized in solution by bulky organic

ligands, which can block access to active catalytic sites and severely hinder the charge transfer between/from NPs in solid films,[74–77] we first assessed the effect of ligand removal from NPs' surface on their electrocatalytic performance. Often the ligand removal from the surface of TMPs is conducted by annealing at high temperatures in a vacuum or hydrogen atmosphere,[5,7] which aside from being energy-intensive can also contaminate the film with carbonaceous residues as well as cause unwanted phase changes and particle fusion, thus severely reducing the surface area and hence the activity of the catalyst.[18,78,79] Since one of our aims was also to compare HER performance of poorly vs well-crystallized NPs, instead, we conducted an NPs' phase transfer from hexane to NMF using HPF_6, which, albeit being much milder, was shown to be effective at the removal of the native ligands from NPs leaving behind positively charged metal sites.[8,9,77,80] As illustrated in **Figure S5** in the Supporting Information, the ligand stripping from the surface of nickel phosphide NPs results in a marked overpotential drop, indicating a notable enhancement of the catalytic performance. This improvement underscores the significance of ligand choice in optimizing electron transfer and, consequently, enhancing the overall catalytic efficiency, hence, we utilized the same protocol for other TMP NP samples.

The efficiency of the ligand-exchange process was monitored with Fourier-transform infrared spectroscopy (FTIR) (**Figure 3**). One can see that prior to ligand exchange, all samples exhibit a group of intensive bands around 2800 – 3000 cm^{-1} corresponding to symmetric and asymmetric vibrations of methyl and methylene units of long alkyl chains.[81] At the same time, we observed no sharp and intensive features at 1500 – 1700 cm^{-1} of carboxylate or carbonyl vibrations,[82] which might have appeared due to the presence of unreacted acylphosphines or by-products of their decomposition, thus suggesting that TOP acts as a sole organic surface ligand. After adding HPF_6 into the biphasic mixture and vigorously shaking it for 10 min the NPs quickly migrated to the NMF layer indicating the removal of organic species from the NPs' surface. Successful ligand stripping is also confirmed by FTIR data, where we observe the complete or nearly complete disappearance of alkyl chain vibration signals (**Figure 3**). Notably, during and after the phase transfer some of the amorphous samples exhibited lower colloidal stability than their crystalline counterparts thus complicating complete ligand stripping even after adding another HPF_6 aliquot, which in turn explains weak residual signals of organic ligands. This can be explained by the less defined surface of amorphous NPs potentially exposing more sites, which poorly adsorb protons or neutralize their charge, thus negating their contribution to colloidal stability. In addition, we further characterized the elemental composition of ligand-stripped NCs using inductively coupled plasma optical emission spectroscopy (ICP-OES). All NCs were found to have a substoichiometric M/P (M = Ni, Co) ratio,

making them relatively phosphorus-rich, most likely due to the removal of metal chloride complexes, which can act as loosely bound Z-type ligands.

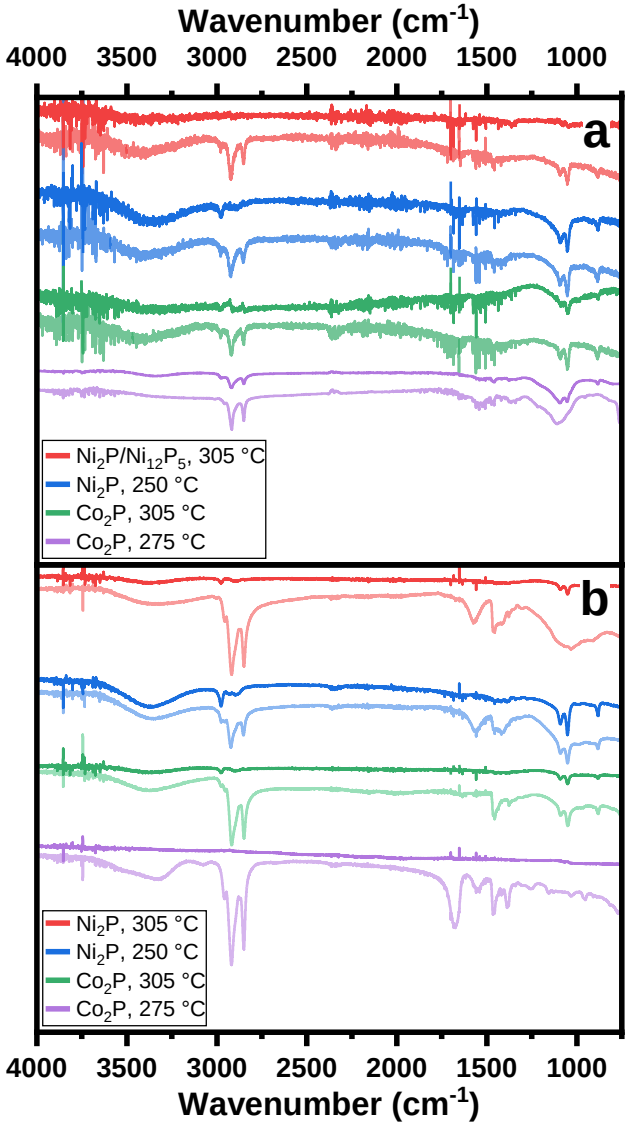

Figure 3. FTIR spectra of nickel and cobalt phosphide NPs synthesized using Bz_3P (a) and $(PrCO)_3P$ (b) before (light lines) and after (darker lines) ligand exchange with HPF_6.

Figure 4 a,b presents the linear sweep voltammetry (LSV) curves of cobalt and nickel phosphide NPs recorded in 0.5 M H_2SO_4 aqueous solution, which exhibit two clear trends. First, the overpotentials of nickel phosphide NPs are lower than those of cobalt phosphide NPs, which can be explained by the lower Gibbs free energy of the adsorbed atomic hydrogen ΔG_{H^*} indicating the ability of the catalyst to release hydrogen and unblock the reactive catalytic sites.[9] Second, the samples with lower crystallinity prepared at lower temperatures demonstrate markedly higher overpotentials than their counterparts prepared at 305 °C with more pronounced crystalline features in XRD patterns, which can be explained by the much higher conductivity of well-crystallized NPs.[83] In the case of high-temperature nickel phosphide NPs synthesized using Bz_3P and $(PrCO)_3P$, overpotentials of only

50 mV and 68 mV, respectively, are required to reach a current density of 10 mA/cm^2, which favorably compares against the reported nickel and cobalt phosphides (see **Table S1** and **Figure S6** in the Supporting Information) and are quite competitive values compared to Pt/C (28 mV) employed as a commercial catalyst.

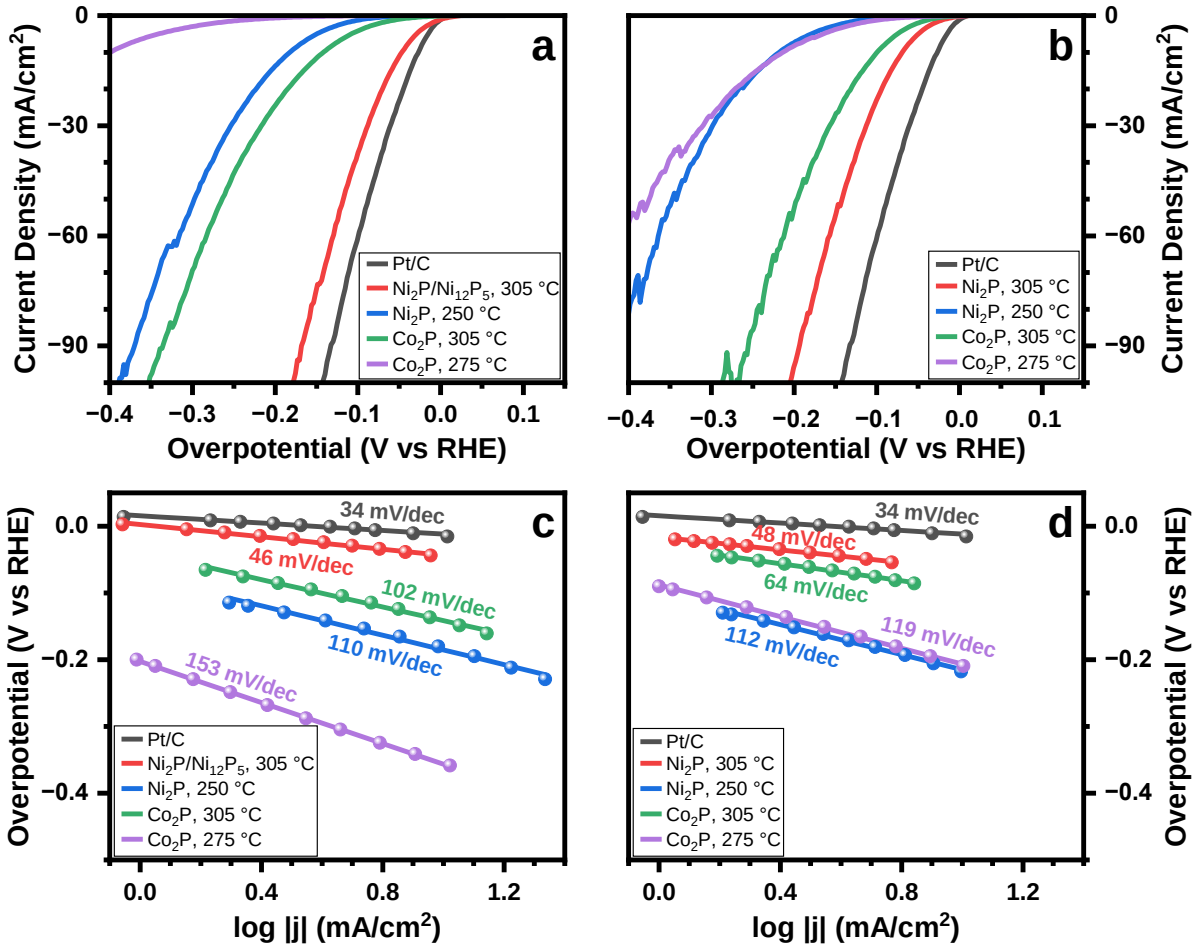

Figure 4. HER-performance of NPs in 0.5 M H_2SO_4: LSV curves (a, b) and Tafel plots (c, d) of the metal phosphide NPs synthesized with Bz_3P (a, c) and $(PrCO)_3P$ (b, d).

Currently, there is limited information in the literature, directly comparing the catalytic performance of amorphous and crystalline nickel and cobalt phosphide NPs, since they can usually be accessed via different synthetic routes, which results in dissimilar compositions, sizes, and structures further complicating proper comparison. In this regard, our work enables the examination of the effect of crystallinity degree on the electrocatalytic performance of TMPs prepared via similar routes and possessing comparable parameters. Although more sophisticated studies, which go beyond the scope of this paper, are needed to properly examine the underlying processes involved in electrocatalysis, we are still able to draw some qualitative conclusions.

In general, amorphous materials are expected to be beneficial for catalysis because they can offer a more flexible composition and structure as well as owing to disorder introducing more defects

and vacancies often presumed to be electrocatalytically active sites.[40,79,84,85] On the other hand, crystalline NPs might exhibit better performance since they possess well-defined facets and some specific crystallographic planes were shown to be particularly active in the reduction of hydrogen.[5,86,87] Furthermore, films of crystalline NPs have higher electrical conductivity, which appears to be the major factor contributing to the better catalytic performance of crystalline NPs compared to amorphous ones.[88]

To further assess the catalytic efficiency, Tafel slope analysis was conducted, serving as an indicator of the reaction kinetics. As illustrated in **Figure 4 c,d**, crystalline nickel phosphide NPs exhibit the smallest Tafel slopes (46 and 48 mV/dec in the case of Bz_3P and $(PrCO)_3P$, respectively) compared to amorphous/poorly crystalline nickel phosphide (112 and 110 mV/dec), crystalline (102 and 64 mV/dec) and amorphous/poorly crystalline (145 and 118 mV/dec) cobalt phosphide NPs. These values do not match the Tafel slope values of 29, 38, and 116 mV/dec expected for particular rate-limiting steps of the Volmer-Heyrovsky-Tafel HER mechanism, which is quite common for non-metal materials.[89] In some publications, values lower than ca. 60 mV/dec are interpreted as a probable signature of a barrierless electron transfer mechanism[90] or a mechanism involving a fast Volmer step followed by the Heyrovsky step determining the overall reaction rate.[7,45] However, more recently it was suggested that such Tafel analysis does not accurately describe electrocatalysis and does not allow conclusive identification of the rate-determining steps possibly due to more complex reaction mechanisms and altered parameter values used in theoretical calculations.[89,91] Nevertheless, a conclusion can be made that smaller Tafel slopes indicate a less hindered HER process with superior charge transfer efficiency and faster reaction kinetics.[41]

Figure 5 presents the LSV curves along with corresponding Tafel plots of cobalt and nickel phosphide NPs recorded in 1 M KOH. In general, HER overpotentials for a variety of electrocatalysts of different nature are significantly higher than those observed in the acidic solutions, most likely due to the overall change of the HER mechanism resulting in more complicated kinetics involving additional water dissociation step.[92] As one can notice, in our case we observe the same trend both in LSV curves and respective Tafel slopes across all studied electrodes pointing to slower reaction rates.

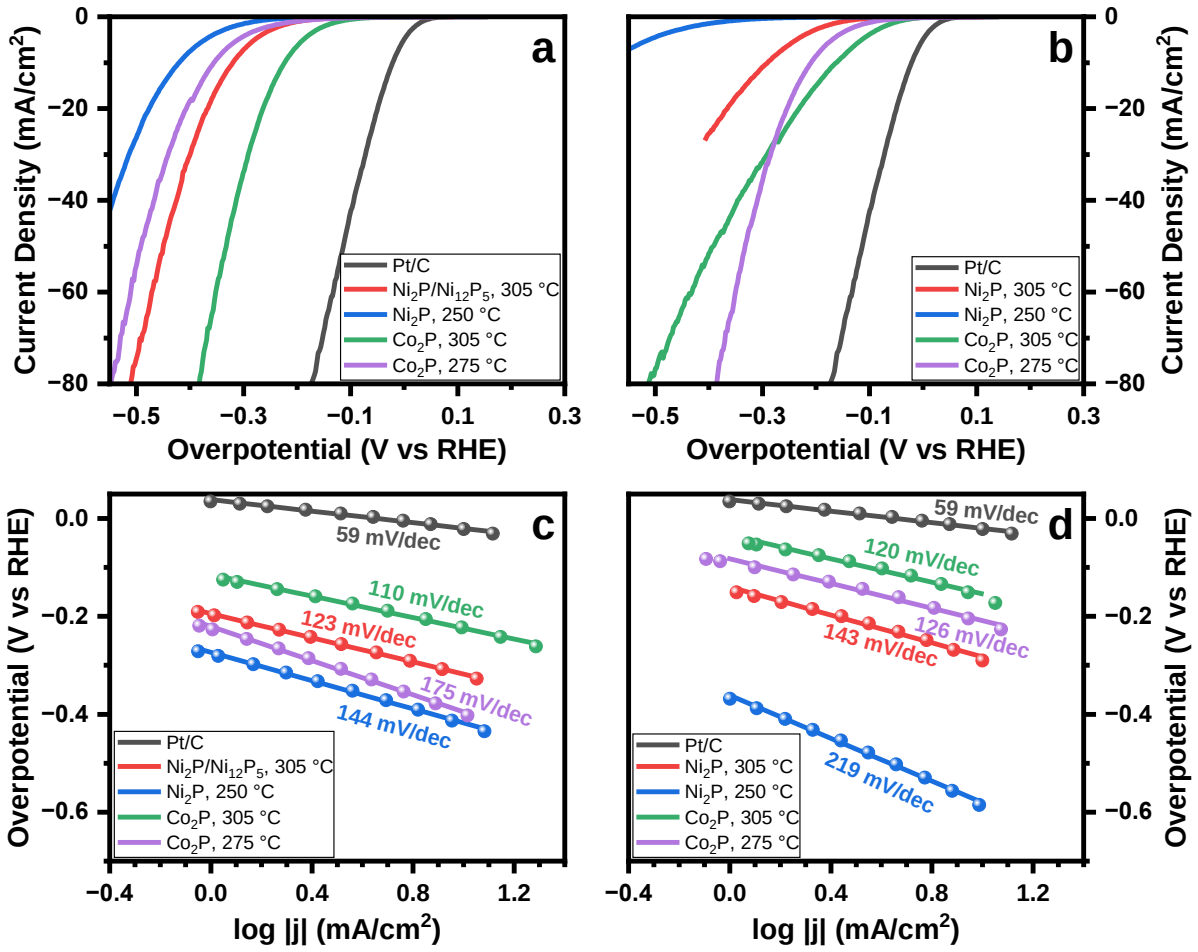

Figure 5. HER-performance of NPs in 1.0 M KOH: LSV curves (a, b) and Tafel plots (c, d) of the metal phosphide NPs synthesized with Bz_3P (a, c) and $(PrCO)_3P$ (b, d).

Similarly to HER in an acidic medium, lower overpotentials were achieved in the case of well-crystallized NPs further supporting our assumption that film conductivity plays an important role in the catalyst activity. Interestingly, in an alkaline medium both types of cobalt phosphide NPs exhibit lower overpotentials, which is in line with previous reports and might be attributed to the different absorbed species involved in the initial reaction steps, their binding affinity to the surface, as well as phase/compositional transformation during the electrocatalysis.[93,94]

3. Conclusion

In this work, we report the application of triacylphosphines as the new type of phosphorus precursors for the synthesis of nickel and cobalt phosphide NPs. We demonstrate that in comparison to alkyl- or arylphosphines with similar structures commonly used for the preparation of TMP NPs, acylphosphines react with metal chlorides at lower temperatures and directly yield metal phosphide NPs without the intermediate metal reduction step, minimizing the contamination of the final product. At the same time, in contrast to other highly reactive phosphorus sources, such as white phosphorus, PH_3, or $P(SiMe_3)_3$, they are relatively safe for use and can be prepared on a large scale using cheap

and widely available starting materials. Acylphosphines react with nickel and cobalt chlorides in the presence of TOP at temperatures as low as 250 °C yielding NPs with sizes < 10 nm, which can later be transformed into crystalline NPs by heating up to 305 °C. Furthermore, under similar synthesis conditions, Bz_3P and $(PrCO)_3P$ react with iron and copper chlorides forming large crystalline particles, while reaction with molybdenum chloride yields small poorly crystalline NPs, demonstrating a great potential of these P-precursors in the synthesis of various metal phosphide nanomaterials. Our method provides access to TMP NPs with different crystallinity expanding the possibility to control physical and electrical properties, which, as demonstrated in this work, determine their performance in electrocatalysis. We examined the HER performance of the synthesized Ni and Co phosphide NPs after ligand stripping using HPF_6 and showed that both types of crystalline NPs demonstrate lower overpotential than their amorphous counterparts. At the same time, in an acidic medium nickel phosphide NPs exhibit significantly better HER performance than cobalt phosphides, reaching overpotentials as low as 50 mV at a current density of 10 mA/cm^2, which is among the lowest overpotentials for this type of materials and can be considered as a competitive value compared with Pt/C (28 mV).

4. Experimental Section/Methods

Materials. Benzoyl chloride (99.5+ %), 1,2-dimethoxyethane (DME, 99+ %, stabilized with butylated hydroxytoluene), hexane (97 %, extra dry), N-methylformamide (NMF, 99 %), sodium (≥ 99.8 %), *tert*-butanol (*t*-BuOH, 99.5 %), tetrahydrofuran (THF, 99.5 %, stabilized, extra dry), and sulfuric acid (95 %) were purchased from Acros. Butyryl chloride (≥ 99 %), cobalt (II) chloride (> 98 %), copper (I) chloride (≥ 99.995 %), ethyl butyrate (99 %), hexafluorophosphoric acid (HPF_6, ~55 wt. % in H_2O), hydrogen peroxide (30 %, trace metal grade), iron (II) chloride (98 %), methyl benzoate (99 %), molybdenum (V) chloride (99.6 %), naphthalene (≥ 99 %), nickel (II) chloride (98 %), 1-octadecene (ODE, technical grade, 90 %), red phosphorus (powder, 99 %), and toluene (anhydrous, 99.8 %) were purchased from Sigma-Aldrich. Tri-*n*-octylphosphine (TOP, 97 %) was purchased from abcr. Methanol (99.8 %), *n*-hexane (≥ 97 %), 2-propanol (99.8 %), acetonitrile (≥ 99.95 %), ethanol (≥ 99.8 %), and nitric acid (≥ 68 %, trace metal grade) were purchased from Fisher Chemical. Deuterochloroform (99.8 *at.* % D, stabilized with Ag) was purchased from Carl Roth. Potassium hydroxide (KOH, 90 %) was purchased from Merck. DME was dried by refluxing over sodium/benzophenone for 2 h under argon followed by distillation under argon.[95] ODE was dried and degassed under vacuum (0.1 mbar) at 90 °C for 3 h. Both solvents were stored in the nitrogen-filled glovebox over 3 Å molecular sieves.

Synthesis of $(PrCO)_3P$ and Bz_3P. Caution! *Synthesis of sodium phosphide involves heating highly reactive compounds in a flammable solvent, which can constitute a fire hazard. In addition,*

sodium phosphide readily reacts with water (including air moisture) and protic solvents (such as alcohols) releasing toxic and explosive phosphine gas.

Prior to use, all glassware was dried at 150 °C for 24 h. All synthesis operations were performed either in a nitrogen-filled glovebox or on a Schlenk line under an argon atmosphere. The acylphosphine synthesis procedure was adapted from ref. [66].

In the nitrogen-filled glovebox, a 100 mL three-neck flask was loaded with 3.1 g (100 mmol) of red phosphorus powder, 2.6 g (20 mmol) of naphthalene, and 80 mL of dry DME. The flask was removed from the glovebox and connected to a Schlenk line with argon atmosphere. Then 8.1 g (350 mmol) of sodium cut into small chunks were added into the flask under argon flow. Afterward, the flask was sealed with silicone septa, heated to 80 °C, and kept stirring at this temperature overnight. During the reaction, the suspension in the flask turned from red to dark green and then black. After the reaction, the flask was cooled to room temperature and the reaction mixture was transferred via a double-tipped cannula into air-tight argon-filled glass centrifuge tubes and centrifuged at 4500 rpm for 10 min. The supernatant was removed via cannula, the precipitate was redispersed in 30 mL of dry DME, and the mixture was centrifuged. The above redispersion-precipitation process was repeated one more time. Finally, the precipitate was redispersed in 300 mL of dry DME and transferred via a double-tipped cannula into a degassed 500 mL three-neck flask under argon.

Then the reaction mixture was cooled down with an ice bath to 0 °C and the solution of 21.2 mL (210 mmol) of *t*-BuOH in 30 mL of DME was slowly added via a syringe pump. After that, the ice bath was removed, and the flask was allowed to warm up to room temperature and kept under vigorous stirring for 2 h. Then the flask was placed in an ice bath and 19.8 mL (150 mmol) of ethyl butyrate or 18.8 mL (150 mmol) of methyl benzoate were added dropwise. The flask was kept at room temperature for 1 h, during which the reaction mixture turned greenish-yellow (in the case of butyrate) or dark red (in the case of benzoate). Afterward, the flask was cooled to 0 °C, and 30.9 mL (300 mmol) of butyryl chloride or 34.9 mL (300 mmol) of benzoyl chloride were slowly added dropwise. ***Note:*** *The reaction is fairly exothermic, thus the rate of addition should be controlled to avoid rapid temperature rise.* The reaction mixture was left under vigorous stirring overnight whilst the reaction mixture turned yellowish-grey (in the case of $(PrCO)_3P$) or yellow (in the case of Bz_3P). ***Note:*** *If the reaction mixture becomes too viscous it can be further diluted with dry DME or THF*. After that, the solids were removed from the reaction mixture by centrifugation under an argon atmosphere yielding a transparent solution. Then all volatiles were evaporated from the reaction mixture under vacuum resulting in yellow oil ($(PrCO)_3P$) or bright yellow powder (Bz_3P).

To purify $(PrCO)_3P$, the reaction product was diluted two times with hexane, centrifuged under argon to remove remaining solids, and then kept under a vacuum on a Schlenk line at 30 °C for 8 h. For the purification of Bz_3P, the reaction product was dissolved under an inert atmosphere in 100 mL of dry THF and then precipitated by adding ca. 300 mL of dry hexane. The solid was isolated by centrifugation and recrystallized one more time as described in the previous sentence. Finally, the solid product was dried under a vacuum at room temperature for 8 h.

$(PrCO)_3P$: **^{1}H NMR** (300 MHz, $CDCl_3$, δ) 2.86 (td, J = 7.2, 1.7 Hz, 6H, CH_2-CO), 1.64 (h, J = 7.3 Hz, 6H, CH_3-CH_2), 0.93 (t, J = 7.4 Hz, 9H, CH_3). **^{13}C NMR** (75 MHz, $CDCl_3$, δ) 215.2 (d, $^1J_{PC}$ = 49.3 Hz, *C*=O), 50.8 (d, *C*H_2-CO, $^2J_{PC}$ = 30.9 Hz), 17.2 (d, CH_3-*C*H_2 $^3J_{PC}$ = 3.6 Hz), 13.5 (CH_3, s). **^{31}P NMR** (121 MHz, $CDCl_3$, δ) 61.3 (s). Anal. calcd for $C_{12}H_{21}O_3P$: C 59.00, H 8.67; found: C 58.70, H 8.86.

Bz_3P: **^{1}H NMR** (300 MHz, $CDCl_3$, δ) 8.05 – 7.95 (m, 6H, *o*-H), 7.65 – 7.56 (m, 3H, *p*-H), 7.53 – 7.45 (m, 6H, *m*-H). **^{13}C NMR** (75 MHz, $CDCl_3$, δ) 206.0 (d, $^1J_{PC}$ = 33.3 Hz, *C*=O), 140.2 (d, $^2J_{PC}$ = 34.6 Hz, C_{ipso}), 134.2 (d, J = 1.4 Hz, C_{para}), 129.0 – 128.6 (m, C_{arom}). **^{31}P NMR** (121 MHz, $CDCl_3$, δ) 54.0 (s). Anal. calcd for $C_{21}H_{15}O_3P$: C 72.82, H 4.37; found: C 72.88; H 4.28.

Synthesis of nickel, cobalt, iron, copper, and molybdenum phosphide NPs. In a typical synthesis, 0.5 mmol of metal chloride were mixed with 900 µL of TOP (2 mmol) and 5 mL of dry degassed ODE in a three-neck 25 mL flask in a nitrogen-filled glovebox. The obtained mixture was transferred to a Schlenk line, heated under argon flow to 170 °C, and maintained at this temperature for 15 min to dissolve the metal precursor. After that, the solution was cooled to 90 °C, degassed under vacuum (0.1 mbar) for 30 min, and then purged with argon. In parallel, in a nitrogen-filled glovebox, a phosphorus precursor solution was prepared by dissolving either 67.5 µL (0.25 mmol) of $(PrCO)_3P$ in 1 mL of dry degassed ODE or 86.5 mg of Bz_3P (0.25 mmol) in 1 mL of anhydrous toluene. Next, the obtained solution was injected into the metal precursor solution, and the flask was evacuated for 5 min to remove the solvent. Then, the mixture was quickly heated to the required temperature (250 °C, 275 °C, or 305 °C) and kept for 25 min (in the case of molybdenum phosphide for 2 h) for the nucleation and growth of NPs. Finally, the reaction mixture was cooled to room temperature, and NPs were purified by multiple precipitation and redispersion steps, using a 2-propanol/methanol mixture (2:1) and hexane.

Ligand stripping. The ligands were removed by adding 4 mL of NMF and 10 µL of ~55 *wt.* % HPF_6 aqueous solution to a 4 mL solution of NPs in hexane. The mixture was vigorously stirred for 30 min followed by adding 10 µL of HPF_6 solution and stirring for 30 min. Afterward, the hexane layer was discarded, and NPs were purified by the multiple precipitations with a toluene/acetonitrile

mixture (5:1) and redispersing in NMF. Finally, the NPs were redispersed in ethanol and stored prior to the electrocatalytic tests.

Characterization. ^{1}H, ^{13}C, and ^{31}P NMR spectroscopy was performed using Bruker Avance III 600 spectrometer. For the measurements, acylphosphines (ca. 5 *w/v* %) were dissolved in deuterochloroform in the nitrogen-filled glovebox and transferred into air-tight NMR tubes. Elemental analysis (CHNS) was done with FlashSmart Elemental Analyzer. Bright-field TEM imaging was performed on a JEOL JEM-1400 Plus microscope operated at 120 kV. Powder XRD patterns were acquired using a Bruker D2 Phaser equipped with an X-ray tube with a Cu anode operated at 30 kV and 10 mA. WinXPow software with references from the Inorganic Crystal Structure Database (ICSD) was used for the phase analysis. For the measurements, concentrated hexane solutions of metal phosphide NPs were drop-cast on a Si wafer and dried under air. FTIR measurements were performed on a Nicolet 8700 FTIR spectrometer using the attenuated total reflectance method.

The elemental composition of NPs was determined by ICP-OES using an iCAP 7000 Series (Thermo Scientific). For the measurements, aliquots of ligand-exchanged NCs were transferred into HDPE centrifugation tubes, dried, and then decomposed using 30 % hydrogen peroxide and concentrated nitric acid according to the protocol from ref. [96] for 24 h. Shortly before the analysis samples were diluted to 15 mL with Milli-Q water and measurements were carried out in triplicate for each sample.

Electrochemical tests were conducted using a three-electrode setup (Metrohm Autolab) to characterize the catalytic performance of the synthesized materials. The experimental arrangement comprised a reference electrode, a counter electrode, and a working electrode. For the experiments conducted in 0.5 M H_2SO_4, an Ag/AgCl electrode in saturated KCl was employed as the reference electrode. For experiments in 1 M KOH, a Hg/HgO electrode served as the reference electrode. A graphite rod was utilized as the counter electrode. A glassy carbon disk electrode, with a diameter of 3 mm and a geometric area of 0.07 cm^2 was used as a working electrode. The NP films were deposited by drop-casting aliquots of the ethanol dispersions of ligand-stripped NPs onto the glassy carbon electrode to get an average mass loading of 0.5 – 0.7 mg/cm^2. After drying in ambient air, a stable and uniform catalyst layer on the electrode surface was formed. The electrochemical measurements were conducted through linear sweep voltage scans initiated from -0.4 to 0 V in 0.5 M H_2SO_4 and -0.6 to 0 V in 1 M KOH vs. the reversible hydrogen electrode (RHE) with a scan rate of 5 mVs^{-1}.

SUPPORTING INFORMATION

^{1}H, ^{13}C, and ^{31}P NMR spectra of the acylphosphines, additional TEM images, XRD, ICP-OES, and electrochemistry data. Supporting Information is available from the Wiley Online Library or from the authors.

Corresponding authors

artsiom.antanovich@pci.uni-hannover.de, vladimir.lesnyak@tu-dresden.de

Conflict of Interest

The authors declare no conflict of interest.

Keywords:

Phosphides, electrocatalysis, hydrogen evolution reaction, water splitting, nanoparticles

ACKNOWLEDGMENTS

A.A. acknowledges funding from the European Union's Horizon 2020 research and innovation programme under the Marie Sklodowska-Curie grant agreement No 101031243. V.S., P.K., A.I., and V.L. thank the German Research Foundation for funding through CRC 1415, EY 16/30-1, and RTG 2767 projects. We are grateful to Heike Trepte and Anett Rudolph for the elemental analysis and NMR spectroscopy of acylphosphines. The authors are grateful to Christine Steinbach (Leibniz-Institut für Polymerforschung, Dresden) for ICP-OES measurements.

REFERENCES

[1] G. Li, Y. Feng, Y. Yang, X. Wu, X. Song, L. Tan, *Nano Mater. Sci.* **2024**, *6*, 174.

[2] S. S. Patil, P. S. Patil, *Nanoscale* **2022**, *14*, 16731.

[3] J.-H. Pöhls, A. Faghaninia, G. Petretto, U. Aydemir, F. Ricci, G. Li, M. Wood, S. Ohno, G. Hautier, G. J. Snyder, G.-M. Rignanese, A. Jain, M. A. White, *J. Mater. Chem. C* **2017**, *5*, 12441.

[4] G. Chang, Y. Zhao, L. Dong, D. P. Wilkinson, L. Zhang, Q. Shao, W. Yan, X. Sun, J. Zhang, *J. Mater. Chem. A* **2020**, *8*, 4996.

[5] E. J. Popczun, J. R. McKone, C. G. Read, A. J. Biacchi, A. M. Wiltrout, N. S. Lewis, R. E. Schaak, *J. Am. Chem. Soc.* **2013**, *135*, 9267.

[6] S. Cao, Y. Chen, C.-J. Wang, P. He, W.-F. Fu, *Chem. Commun.* **2014**, *50*, 10427.

[7] Y. Pan, Y. Liu, J. Zhao, K. Yang, J. Liang, D. Liu, W. Hu, D. Liu, Y. Liu, C. Liu, *J. Mater. Chem. A* **2015**, *3*, 1656.

[8] J. Liu, M. Meyns, T. Zhang, J. Arbiol, A. Cabot, A. Shavel, *Chem. Mater.* **2018**, *30*, 1799.

[9] J. Liu, Z. Wang, J. David, J. Llorca, J. Li, X. Yu, A. Shavel, J. Arbiol, M. Meyns, A. Cabot, *J. Mater. Chem. A* **2018**, *6*, 11453.

[10] H. P. Andaraarachchi, M. J. Thompson, M. A. White, H.-J. Fan, J. Vela, *Chem. Mater.* **2015**, *27*, 8021.

[11] S. Zhang, E. Ye, S. Liu, S. H. Lim, S. Y. Tee, Z. Dong, M. Han, *Adv. Mater.* **2012**, *24*, 4369.

[12] E. J. Popczun, C. G. Read, C. W. Roske, N. S. Lewis, R. E. Schaak, *Angew. Chemie Int. Ed.* **2014**, *53*, 5427.

[13] J. F. Callejas, C. G. Read, E. J. Popczun, J. M. McEnaney, R. E. Schaak, *Chem. Mater.* **2015**, *27*, 3769.

[14] J. F. Callejas, J. M. McEnaney, C. G. Read, J. C. Crompton, A. J. Biacchi, E. J. Popczun, T. R. Gordon, N. S. Lewis, R. E. Schaak, *ACS Nano* **2014**, *8*, 11101.

[15] D. Y. Chung, S. W. Jun, G. Yoon, H. Kim, J. M. Yoo, K.-S. Lee, T. Kim, H. Shin, A. K. Sinha, S. G. Kwon, K. Kang, T. Hyeon, Y.-E. Sung, *J. Am. Chem. Soc.* **2017**, *139*, 6669.

[16] Y. Park, H. Kang, Y. Hong, G. Cho, M. Choi, J. Cho, D.-H. Ha, *Int. J. Hydrogen Energy* **2020**, *45*, 32780.

[17] F. D'Accriscio, E. Schrader, C. Sassoye, M. Selmane, R. F. André, S. Lamaison, D. Wakerley, M. Fontecave, V. Mougel, G. Le Corre, H. Grützmacher, C. Sanchez, S. Carenco, *ChemNanoMat* **2020**, *6*, 1208.

[18] J. M. McEnaney, J. C. Crompton, J. F. Callejas, E. J. Popczun, A. J. Biacchi, N. S. Lewis, R. E. Schaak, *Chem. Mater.* **2014**, *26*, 4826.

[19] X. Zhang, X. Yu, L. Zhang, F. Zhou, Y. Liang, R. Wang, *Adv. Funct. Mater.* **2018**, *28*, 1706523.

[20] R. Ge, J. Huo, T. Liao, Y. Liu, M. Zhu, Y. Li, J. Zhang, W. Li, *Appl. Catal. B Environ.* **2020**, *260*, 118196.

[21] L. De Trizio, A. Figuerola, L. Manna, A. Genovese, C. George, R. Brescia, Z. Saghi, R. Simonutti, M. Van Huis, A. Falqui, *ACS Nano* **2012**, *6*, 32.

[22] L. De Trizio, R. Gaspari, G. Bertoni, I. Kriegel, L. Moretti, F. Scotognella, L. Maserati, Y. Zhang, G. C. Messina, M. Prato, S. Marras, A. Cavalli, L. Manna, *Chem. Mater.* **2015**, *27*, 1120.

[23] X. Li, J. Zhang, Y. Zhang, R. Zhang, D. Chen, C. Zhang, X. Zhang, B. Wang, H. Q. Luo, N. B. Li, *Int. J. Hydrogen Energy* **2020**, *45*, 21422.

[24] A. S. Sabir, E. Pervaiz, R. Khosa, U. Sohail, *RSC Adv.* **2023**, *13*, 4963.

[25] S. C. Perera, G. Tsoi, L. E. Wenger, S. L. Brock, *J. Am. Chem. Soc.* **2003**, *125*, 13960.

[26] K. A. Gregg, S. C. Perera, G. Lawes, S. Shinozaki, S. L. Brock, *Chem. Mater.* **2006**, *18*, 879.

[27] Q. Deng, X. Dong, P. K. Shen, J. Zhu, *Adv. Sci.* **2023**, *10*, 2207470.

[28] Z. Pu, Q. Liu, A. M. Asiri, X. Sun, *ACS Appl. Mater. Interfaces* **2014**, *6*, 21874.

[29] L. Hong, R. Guo, Y. Yuan, X. Ji, Z. Lin, Z. Li, W. Pan, *ChemSusChem* **2021**, *14*, 539.

[30] S. Cao, C. Wang, W. Fu, Y. Chen, *ChemSusChem* **2017**, *10*, 4306.

[31] S. T. Oyama, *J. Catal.* **2003**, *216*, 343.

[32] S. Fujita, K. Nakajima, J. Yamasaki, T. Mizugaki, K. Jitsukawa, T. Mitsudome, *ACS Catal.* **2020**, *10*, 4261.

[33] T. Tsuda, M. Sheng, H. Ishikawa, S. Yamazoe, J. Yamasaki, M. Hirayama, S. Yamaguchi, T. Mizugaki, T. Mitsudome, *Nat. Commun.* **2023**, *14*, 5959.

[34] S. Yamaguchi, S. Fujita, K. Nakajima, S. Yamazoe, J. Yamasaki, T. Mizugaki, T. Mitsudome, *Green Chem.* **2021**, *23*, 2010.

[35] C. A. Downes, N. J. Libretto, A. E. Harman-Ware, R. M. Happs, D. A. Ruddy, F. G. Baddour, J. R. Ferrell, S. E. Habas, J. A. Schaidle, *ACS Appl. Energy Mater.* **2020**, *3*, 10435.

[36] K. U. D. Calvinho, A. B. Laursen, K. M. K. Yap, T. A. Goetjen, S. Hwang, N. Murali, B. Mejia-Sosa, A. Lubarski, K. M. Teeluck, E. S. Hall, E. Garfunkel, M. Greenblatt, G. C. Dismukes, *Energy Environ. Sci.* **2018**, *11*, 2550.

[37] L. Ji, L. Li, X. Ji, Y. Zhang, S. Mou, T. Wu, Q. Liu, B. Li, X. Zhu, Y. Luo, X. Shi, A. M. Asiri, X. Sun, *Angew. Chemie Int. Ed.* **2020**, *59*, 758.

[38] X. Liu, C. Cui, S. Wei, J. Han, X. Zhu, Q. Ge, H. Wang, *Green Chem.* **2023**, *26*, 531.

[39] K. U. D. Calvinho, A. W. Alherz, K. M. K. Yap, A. B. Laursen, S. Hwang, Z. J. L. Bare, Z. Clifford, C. B. Musgrave, G. C. Dismukes, *J. Am. Chem. Soc.* **2021**, *143*, 21275.

[40] Y. Li, Z. Dong, L. Jiao, *Adv. Energy Mater.* **2020**, *10*, 1902104.

[41] Y. Shi, B. Zhang, *Chem. Soc. Rev.* **2016**, *45*, 1529.

[42] T. Aziz, M. A. Haque, S. Saha, B. Mondal, S. Jain, A. Dutta, *Energy & Fuels* **2023**, *37*, 18291.

[43] J. Xu, J. Li, D. Xiong, B. Zhang, Y. Liu, K.-H. Wu, I. Amorim, W. Li, L. Liu, *Chem. Sci.* **2018**, *9*, 3470.

[44] B. You, N. Jiang, M. Sheng, M. W. Bhushan, Y. Sun, *ACS Catal.* **2016**, *6*, 714.

[45] J. Joo, T. Kim, J. Lee, S. Choi, K. Lee, *Adv. Mater.* **2019**, *31*, 1806682.

[46] J. F. Callejas, C. G. Read, C. W. Roske, N. S. Lewis, R. E. Schaak, *Chem. Mater.* **2016**, *28*, 6017.

[47] D. Wu, B. Liu, R. Li, D. Chen, W. Zeng, H. Zhao, Y. Yao, R. Qin, J. Yu, L. Chen, J. Zhang, B. Li, S. Mu, *Small* **2023**, *19*, 2300030.

[48] D. Chen, H. Bai, J. Zhu, C. Wu, H. Zhao, D. Wu, J. Jiao, P. Ji, S. Mu, *Adv. Energy Mater.* **2023**, *13*, 2300499.

[49] P. Xiao, W. Chen, X. Wang, *Adv. Energy Mater.* **2015**, *5*, 1500985.

[50] M. Zeng, Y. Li, *J. Mater. Chem. A* **2015**, *3*, 14942.

[51] H. Bai, D. Chen, Q. Ma, R. Qin, H. Xu, Y. Zhao, J. Chen, S. Mu, *Electrochem. Energy Rev.* **2022**, *5*, 24.

[52] S. Carenco, D. Portehault, C. Boissière, N. Mézailles, C. Sanchez, *Chem. Rev.* **2013**, *113*, 7981.

[53] S. Han, Y. Feng, F. Zhang, C. Yang, Z. Yao, W. Zhao, F. Qiu, L. Yang, Y. Yao, X. Zhuang, X. Feng, *Adv. Funct. Mater.* **2015**, *25*, 3899.

[54] T. I. Korányi, *Appl. Catal. A Gen.* **2003**, *239*, 253.

[55] C. A. Downes, K. M. Van Allsburg, S. A. Tacey, K. A. Unocic, F. G. Baddour, D. A. Ruddy, N. J. LiBretto, M. M. O'Connor, C. A. Farberow, J. A. Schaidle, S. E. Habas, *Chem. Mater.* **2022**, *34*, 6255.

[56] S. E. Habas, F. G. Baddour, D. A. Ruddy, C. P. Nash, J. Wang, M. Pan, J. E. Hensley, J. A. Schaidle, *Chem. Mater.* **2015**, *27*, 7580.

[57] A. G. Rachkov, A. M. Schimpf, *Chem. Mater.* **2021**, *33*, 1394.

[58] A. Ropp, S. Carenco, *Inorg. Chem.* **2024**, *63*, 17077.

[59] M. E. Mundy, D. Ung, N. L. Lai, E. P. Jahrman, G. T. Seidler, B. M. Cossairt, *Chem. Mater.* **2018**, *30*, 5373.

[60] Z. Liu, H. Mu, S. Xiao, R. Wang, Z. Wang, W. Wang, Y. Wang, X. Zhu, K. Lu, H. Zhang, S. Lee, Q. Bao, W. Ma, *Adv. Mater.* **2016**, *28*, 3535.

[61] S. Carenco, I. Resa, X. Le Goff, P. Le Floch, N. Mézailles, *Chem. Commun.* **2008**, 2568.

[62] S. Carenco, Y. Hu, I. Florea, O. Ersen, C. Boissière, N. Mézailles, C. Sanchez, *Chem. Mater.* **2012**, *24*, 4134.

[63] C. Y. Son, I. H. Kwak, Y. R. Lim, J. Park, *Chem. Commun.* **2016**, *52*, 2819.

[64] A. Dutta, S. K. Dutta, S. K. Mehetor, I. Mondal, U. Pal, N. Pradhan, *Chem. Mater.* **2016**, *28*, 1872.

[65] D. J. Scott, J. Cammarata, M. Schimpf, R. Wolf, *Nat. Chem.* **2021**, *13*, 458.

[66] E. Schrader, Synthesis and Properties of Acylphosphines, ETH Zurich, **2018**.

[67] E. Muthuswamy, G. H. L. Savithra, S. L. Brock, *ACS Nano* **2011**, *5*, 2402.

[68] J. Wang, A. C. Johnston-Peck, J. B. Tracy, *Chem. Mater.* **2009**, *21*, 4462.

[69] R.-K. Chiang, R.-T. Chiang, *Inorg. Chem.* **2007**, *46*, 369.

[70] A. E. Henkes, Y. Vasquez, R. E. Schaak, *J. Am. Chem. Soc.* **2007**, *129*, 1896.

[71] G. Becker, M. Rössler, G. Uhl, *Zeitschrift für Anorg. und Allg. Chemie* **1982**, *495*, 73.

[72] E. Vedejs, S. T. Diver, *J. Am. Chem. Soc.* **1993**, *115*, 3358.

[73] R. Ahmad, L. Zdražil, S. Kalytchuk, A. Naldoni, A. L. Rogach, P. Schmuki, R. Zboril, Š. Kment, *ACS Appl. Mater. Interfaces* **2021**, *13*, 47845.

[74] D. Alba-Molina, A. R. Puente Santiago, J. J. Giner-Casares, E. Rodríguez-Castellón, M. T. Martín-Romero, L. Camacho, R. Luque, M. Cano, *J. Mater. Chem. A* **2019**, *7*, 20425.

[75] K. Senevirathne, A. W. Burns, M. E. Bussell, S. L. Brock, *Adv. Funct. Mater.* **2007**, *17*, 3933.

[76] D. Ung, B. M. Cossairt, *ACS Appl. Energy Mater.* **2019**, *2*, 1642.

[77] A. Nag, M. V. Kovalenko, J. Lee, W. Liu, B. Spokoyny, D. V. Talapin, *J. Am. Chem. Soc.* **2011**, *133*, 10612.

[78] W. Liu, V. Srivastava, J. M. Kurley, C. Jiang, D. V. Talapin, *J. Phys. Chem. C* **2022**, *126*, 21136.

[79] G. Liu, F. Hou, S. Peng, X. Wang, B. Fang, *Nanomaterials* **2022**, *12*, 2935.

[80] D. Bandyopadhyay, S. Ghosh, L. Houben, R. Bar-Ziv, M. Bar-Sadan, *ACS Appl. Energy Mater.* **2023**, *6*, 10987.

[81] D. Lin-Vien, N. B. Colthup, W. G. Fateley, J. G. Grasselli, *The Handbook of Infrared and Raman Characteristic Frequencies of Organic Molecules*, Academic Press, San Diego, **1991**.

[82] K. Nakamoto, *Infrared and Raman Spectra of Inorganic and Coordination Compounds*, Wiley-Interscience, New York, **1978**.

[83] C. Wang, L. Chai, X. Cui, Z. Zhou, S. Liu, *J. Phys. Chem. C* **2021**, *125*, 21443.

[84] R. Beltrán-Suito, P. W. Menezes, M. Driess, *J. Mater. Chem. A* **2019**, *7*, 15749.

[85] H.-M. Zhang, J.-J. Wang, Y. Meng, J. Sun, *Int. J. Hydrogen Energy* **2022**, *47*, 36084.

[86] G. Hu, Q. Tang, D. Jiang, *Phys. Chem. Chem. Phys.* **2016**, *18*, 23864.

[87] J. Mou, Y. Gao, J. Wang, J. Ma, H. Ren, *RSC Adv.* **2019**, *9*, 11755.

[88] A. Eftekhari, *Int. J. Hydrogen Energy* **2017**, *42*, 11053.

[89] T. Shinagawa, A. T. Garcia-Esparza, K. Takanabe, *Sci. Rep.* **2015**, *5*, 13801.

[90] I. Paseka, *Electrochim. Acta* **1995**, *40*, 1633.

[91] F. Bellato, M. Ferri, A. Annamalai, M. Prato, L. Leoncino, R. Brescia, L. De Trizio, L. Manna, *ACS Appl. Energy Mater.* **2023**, *6*, 151.

[92] N. Mahmood, Y. Yao, J. Zhang, L. Pan, X. Zhang, J. Zou, *Adv. Sci.* **2018**, *5*, 1700464.

[93] C. G. Read, J. F. Callejas, C. F. Holder, R. E. Schaak, *ACS Appl. Mater. Interfaces* **2016**, *8*, 12798.

[94] R. Zhang, X. Wang, S. Yu, T. Wen, X. Zhu, F. Yang, X. Sun, X. Wang, W. Hu, *Adv. Mater.* **2017**, *29*, 1605502.

[95] R. Inoue, M. Yamaguchi, Y. Murakami, K. Okano, A. Mori, *ACS Omega* **2018**, *3*, 12703.

[96] C. Morrison, H. Sun, Y. Yao, R. A. Loomis, W. E. Buhro, *Chem. Mater.* **2020**, *32*, 1760.